ACS chemical biology

Articles

pubs.acs.org/acschemicalbiology

Small Molecule Regulation of Protein Conformation by Binding in the Flap of HIV Protease

Theresa Tiefenbrunn,*[,†] Stefano Forli,[†] Michael M. Baksh,[‡] Max W. Chang,[§] Meaghan Happer,[∥] Ying-Chuan Lin,[∥] Alexander L. Perryman,[†] Jin-Kyu Rhee,[‡] Bruce E. Torbett,[§] Arthur J. Olson,[†] John H. Elder,[∥] M. G. Finn,[‡] and C. David Stout[†]

[†]Deparatment of Integrative Structural and Computational Biology, [‡]Department of Chemistry, [§]Department of Molecular and Experimental Medicine, [∥]Department of Immunology and Microbial Science, The Scripps Research Institute, 10550 N. Torrey Pines Rd., La Jolla, California 92037, United States

Supporting Information

ABSTRACT: The fragment indole-6-carboxylic acid (1F1), previously identified as a flap site binder in a fragment-based screen against HIV protease (PR), has been cocrystallized with pepstatin-inhibited PR and with apo-PR. Another fragment, 3-indolepropionic acid (1F1-N), predicted by AutoDock calculations and confirmed in a novel inhibition of nucleation crystallization assay, exploits the same interactions in the flap site in two crystal structures. Both 1F1 and 1F1-N bind to the closed form of apo-PR and to pepstatin:PR. In solution, 1F1 and 1F1-N raise the T_m of apo-PR by 3.5−5 °C as assayed by differential scanning fluorimetry (DSF) and show equivalent low-micromolar binding constants to both apo-PR and pepstatin:PR, assayed by backscattering interferometry (BSI). The observed signal intensities in BSI are greater for each fragment upon binding to apo-PR than to pepstatin-bound PR, consistent with greater conformational change in the former binding event. Together, these data indicate that fragment binding in the flap site favors a closed conformation of HIV PR.

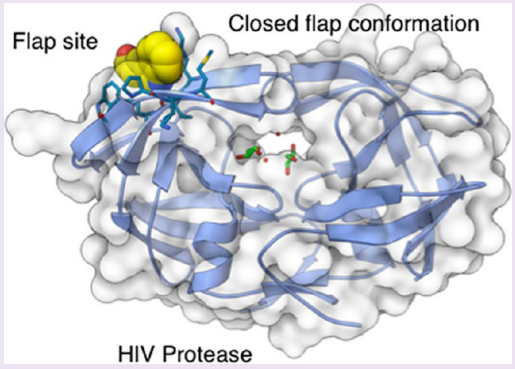

HIV is no longer the rapid death sentence it once was due to the advent of drug therapies including HAART (highly active antiretroviral therapy). However, drug resistance is an increasing problem. It is estimated that 14% of new HIV infections in the United States occur with strains of HIV that are already resistant to one or more of the components of HAART, of which 4.5% represents drug resistance to protease inhibitors.[1] While new therapeutics, vaccines, and/or microbicides being developed to prevent HIV infection may significantly decrease the incidence of this devastating disease in the future, such therapies do not address the problem of resistance for the 33 million people[2] currently living with HIV.

Of the components in the HAART cocktail, HIV protease (PR) inhibitors have been shown to have the best dose−response behavior.[3] However, HIV often develops resistance to PR inhibitors both through mutations in the protease and mutations in processing sites on the gag polyprotein.[4] Eight of the nine FDA approved active site inhibitors are based on the same hydroxyethylene core, with only tipranavir being different. Only darunavir has a different resistance profile compared to the other approved PR inhibitors, and the differences are slight.[5] To overcome resistance, drugs with novel mechanisms of action are required.

Allosteric inhibitors are an attractive alternative to active site inhibitors, particularly for systems prone to developing resistance mutations. Combinations of allosteric inhibitors and active site inhibitors can be even more effective, such as the combination of non-nucleoside reverse transcriptase inhibitors (NNRTIs) and active site nucleoside analogue reverse transcriptase inhibitors (NRTIs) for HIV-1. When administered alone, HIV rapidly develops resistance to NRTIs. However, when a combination of an NRTI, such as azidothymidine (AZT), and an allosteric NNRTI is administered, the evolution of resistance to both drugs is suppressed.[6] An advantage of an allosteric inhibitor is that it will not be subject to the same cross-resistance pressures shared by all active-site inhibitors.[7] This may be the case for darunavir, a PR inhibitor that binds both to the active site and a secondary site near the flap site of HIV-1 protease. Darunavir remains effective against PR mutants that are resistant to other protease inhibitors, perhaps because of the alternative binding site on the protein surface for the S-enantiomer,[8−10] in combination with the strong interactions of darunavir with the PR main chain and favorable occupation of the PR substrate envelope.[11,12] In addition, the dynamic biomechanical relationships that allosteric inhibitors could exploit raise the genetic barrier for mutations that maintain sufficient catalytic efficiency for virus replication.[13] Co-administration of allosteric and

Received: November 10, 2012
Accepted: March 16, 2013
Published: March 29, 2013

Table 1. Crystals and Data Collection

protease/ inhibitor	compound	space group	cell dimensions	morphology	crystallization conditions	flaps	resolution data source
NL4-3 TL-3 (3KFR)	1F1	$P2_12_12_1$	28.72 65.57 92.36	blocks	0.5 M KSCN, 0.1 M MES-HCL, pH 5.8, 10% DMSO	closed	1.3 Å SRRL[a]
NL4-3 pepstatin (4EJD)	1F1	$P2_12_12_1$	28.82 65.63 92.93	blocks	0.2 M KBr, 0.2 M KSCN, 0.1 M NaCacodylate pH 6.5, 3% PGA-LM, 10% DMSO, 3% MPD	closed	1.1 Å SSRL
AR-PR (apo) (4EJ8)	1F1	$P2_12_12_1$	28.95 66.53 91.71	long needles	0.1 M Tris pH 7.5, 28% PEG 4K, 10% DMSO	inverted[b]	2.5 Å Bruker
NL4-3 pepstatin (4EJK)	1F1-N	$P2_12_12_1$	28.65 65.79 92.05	rods	1.0 M NaFormate, 0.1 M NaOAc pH 4.6, 10% DMSO	closed	1.8 Å Bruker
AR-PR (apo) (4EJL)	1F1-N	$P2_12_12_1$	28.82 65.91 92.51	small rods	0.8 M NaFormate, 0.1 M NaOAc pH 5.5, 15% PEG4K	closed	2.0 Å Bruker

[a]Ref 16. [b]Inverted = closed conformation of the flaps with reversed handedness.

active-site inhibitors to decrease the evolution of resistance has been demonstrated both *in vitro* and *ex vivo* in the case of ABL kinase, a target for cancer chemotherapy.[14,15] Hence, an allosteric inhibitor to HIV PR could restore the efficacy of active site inhibitors against multidrug-resistant mutants and, in combination with an active site inhibitor, potentially lessen the evolution of resistance.

A previous fragment screen utilizing X-ray crystallography identified a novel binding site on the surface of HIV PR, termed the flap site; two of the 384 fragments screened bound in this site.[16] This site holds much interest as a potential allosteric site for HIV PR, as suggested by the conformational changes observed in the reported crystal structures with compounds 1F1 (indole-6-carboxylic acid) and 2F4 (2-acetyl-benzothiophene), cocrystallized with TL-3-inhibited PR.[16] Here, we report crystal structures with 1F1 bound to both apo-PR and pepstatin:PR, revealing each to be in the closed conformation. Further, we present crystal structures with a 1F1 derivative, 1F1-N (3-indolepropionic acid), bound to the same site in both apo-PR and pepstatin:PR, again with each in the closed conformation. 1F1-N binding was predicted from *in silico* docking calculations against a library of related fragments and selected for cocrystallization based on a novel inhibition of nucleation crystallization screen. 1F1-N recapitulates each of three principle interactions with PR observed for 1F1, even though it binds in a unique orientation. Interaction of 1F1 and 1F1-N with apo-PR and pepstatin:PR in solution was confirmed using differential scanning fluorimetry (DSF) as well as backscattering interferometry (BSI). BSI establishes K_d values for each compound and reveals a greater extent of conformational change when the fragments bind to apo-PR compared to pepstatin:PR.

RESULTS AND DISCUSSION

AutoDock and Inhibition of Nucleation Assay. As a first step to expand the 1F1 fragment hit[16] into a larger molecule, a library of 2499 commercially available compounds with similar structural features was selected and virtually screened against the crystallographic 1F1 binding site using AutoDock 4.2,[17] as described in Methods. From a list of the top 45 hits, 22 were selected for further screening (Supplemental Table 2). Initially, these compounds were screened for cocrystallization under the same conditions that yielded cocrystals with 1F1 bound to PR:pepstatin, but no hits were obtained. An inhibition of nucleation screen was employed to identify compounds affecting the crystallization behavior of HIV PR, indicating potential binding in the flap site or elsewhere on the protease.

The first inhibition of nucleation screen was based on the growth of the semiopen conformation of apo NL4-3 PR in $P4_12_12$ crystals grown in the presence of Mg^{2+} (e.g., PDB_id 2PC0[18]). These crystals nucleate overnight, and crystal growth is compatible with 10% ethanol or methanol, but not 10% DMSO. It was observed that these crystals do not nucleate in the presence of 20 mM 1F1 dissolved in methanol (Supplemental Figure 1). Further trials demonstrated dose-dependence of crystal formation (Supplemental Figure 2). In addition to 1F1, 1F1-F (4-iodo-1*H*-indole-6-carboxylic acid), 1F1-N (3-indolepropionic acid), and 1F1-U (2-(6-chloro-9H-carbazol-2-yl)propanoic acid) inhibited nucleation of the $P4_12_12$ form at 20 mM or saturation. In contrast, similar compounds such as 1F1-A (2,3-dimethyl-indole-6-carboxylic acid) do not inhibit the nucleation of these crystals (Supplemental Table 2), suggesting that the effect is specific for fragments that bind specifically to PR. We postulate that binding in the flap site selects for HIV PR in a closed form, which is incompatible with the semiopen PR conformation in the $P4_12_12$ lattice.[18]

A second inhibition of nucleation assay was developed to overcome the noncompatibility of the $P4_12_12$ crystal form with DMSO, as several of the compounds of interest were only soluble in DMSO. For this assay, $P6_122$ crystals of TL-3-inhibited HIV PR were used (e.g., PDB_id 3KFP[16]). The $P6_122$ crystal form grows readily under a number of conditions, including those containing 10% DMSO, but these crystals shatter and dissolve if incubated with 1F1 and will not grow in its presence (Supplemental Figure 3). In this assay, 1F1-E (3-(carboxymethyl)-1*H*-indole-2,6-dicarboxylic acid), 1F1-H (3-(carboxymethyl)-2-methyl-1*H*-indole-6-carboxylic acid), and 1F1-N inhibited crystal growth completely (Supplemental Table 2). Although the inhibition of nucleation assays are not quantitative and may not be specific for interactions only in the flap site, they allowed further cocrystallization trials to focus on a small subset of fragments. Only 1F1 and 1F1-N inhibited

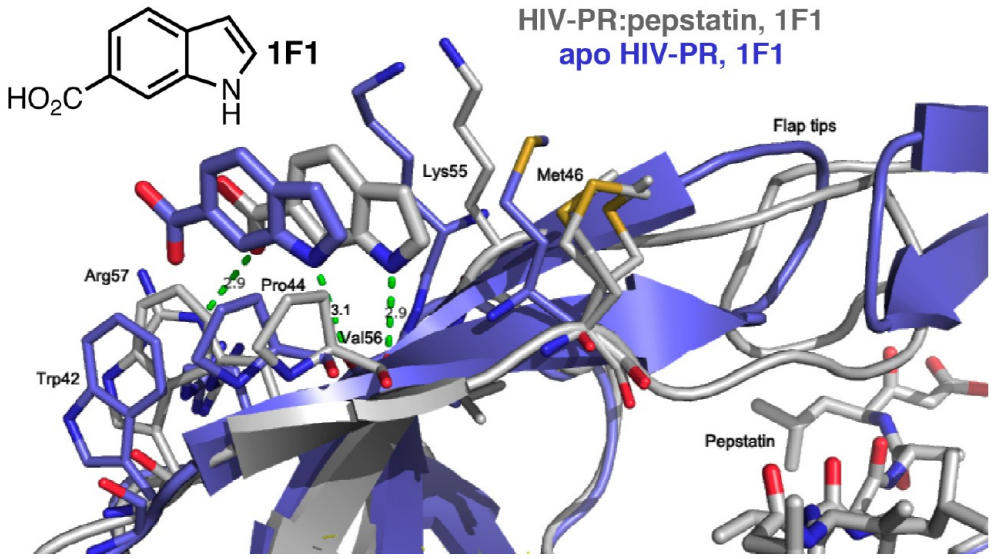

Figure 1. Structure of HIV PR:pepstatin bound to 1F1 (gray) compared to structure of apo HIV PR bound to 1F1 (blue). Note the inverted orientation of the flap tips and the shift of the binding site for the apo−PR complex. Met46 is disordered in the PR:pepstatin structure and adopts three conformations with partial occupancy.

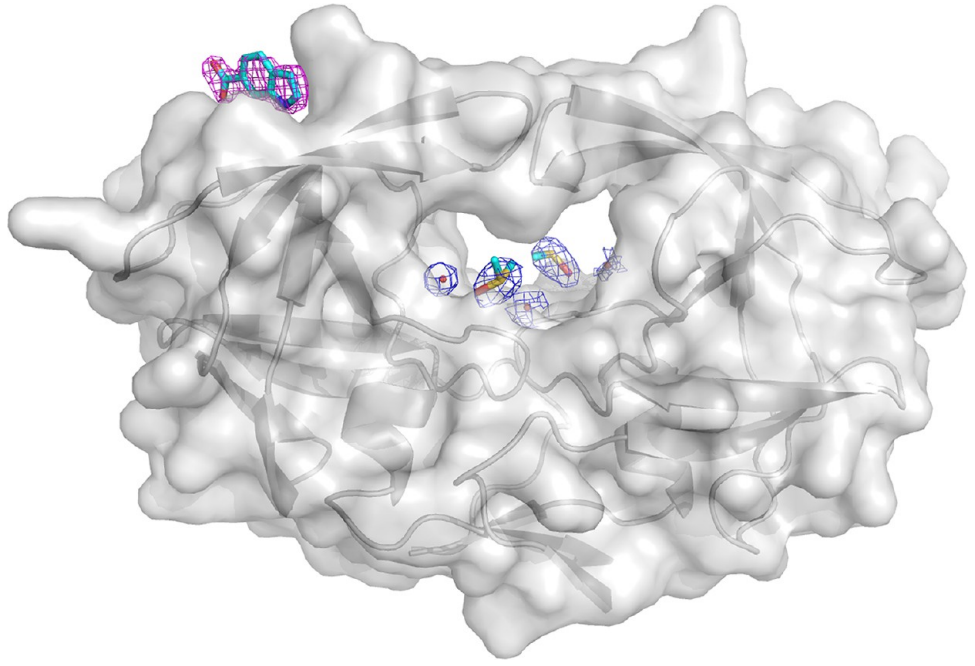

Figure 2. 1F1 and active site electron density for apo-PR with 1F1 bound. Note the absence of peptide-like density in the active site (compare Supplemental Figure 8).

nucleation in both assays, and cocrystals were obtained with 1F1-N bound to apo-PR and pepstatin:PR.

PR:Pepstatin with 1F1. 1F1 was cocrystallized with pepstatin-inhibited HIV PR. Chunky prismatic $P2_12_12_1$ crystals grew under several conditions, and a structure to 1.1 Å resolution was obtained (Table 1; Supplemental Figure 1; Figure 1). Both the crystal form and the 1F1 binding site are similar to the published TL-3-inhibited HIV PR structure (PDB_id 3KFR[16]). One minor difference is in the conformation of Arg57. In 3KFR, Arg57 is 100% flipped to form a hydrogen bonding interaction with the carboxylic acid moiety of 1F1, whereas in the pepstatin-bound structure, Arg57 is only ~50% flipped to bind to 1F1, with the other occupied conformation maintaining the usual hydrogen bonding interaction with Glu35.

Apo-PR with 1F1. Cocrystallization of 1F1 with autolysis-resistant apo-PR (mutations relative to wild-type are Q7K, L33I, L63I, C67A, and C95A[20]) yielded rod-shaped $P2_12_12_1$ crystals, and a structure was obtained at 2.5 Å (Table 1; Supplemental Table 1; Figure 1). This structure of apo-PR with 1F1 is unusual in that the flaps are closed and the active site is not occupied by a peptide or peptidomimetic inhibitor; it is empty aside from two DMSO solvent molecules, one glycerol, and 10 ordered water molecules (Figure 2; compare Supplemental Figure 8a). Another unusual feature of this structure is that the flaps are closed in a conformation with

dx.doi.org/10.1021/cb300611p | ACS Chem. Biol. 2013, 8, 1223−1231

opposite handedness compared to the standard closed conformation of HIV PR. Residues 43−58 of each monomer shift, and the stacking at the tips of the flaps is inverted (Figure 1). A closed conformation of HIV PR with inverted flap tips was first observed in MD simulations,[21] and this conformation of the flaps is commonly observed in semiopen structures of apo-PR,[18] but this is the first time it has been described for a crystal structure with closed flaps. These results suggest that apo-PR in solution adopts a variety of conformations with both conformations of the flap tips represented, and either conformation can be trapped in a crystal lattice. The 1F1 binding site is shifted ∼2.5 Å due to a shift in the flap relative to the structures with pepstatin and TL-3 inhibited PR, but the key interactions of the fragment are maintained (Figure 1). In this crystal form, Arg57 does not flip, but remains hydrogen bonded to Glu35.

Pepstatin:PR with 1F1-N. The structure of 1F1-N bound to pepstatin:PR was obtained from rod-shaped $P2_12_12_1$ crystals to 1.8 Å (Table 1; Supplemental Table 1; Figure 3) and is very

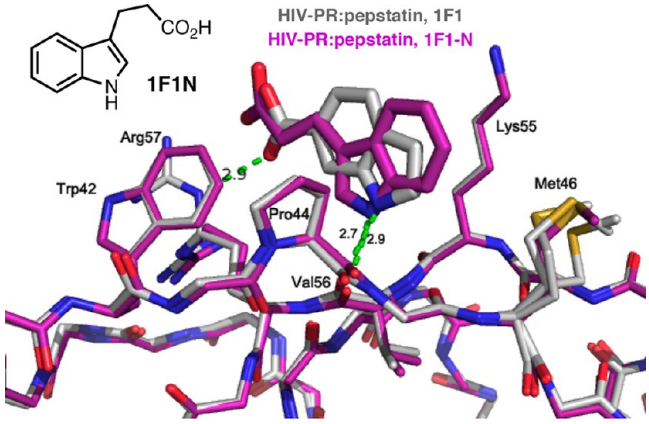

Figure 3. HIV PR:pepstatin bound to 1F1(gray) superposed onto HIV PR:pepstatin bound to 1F1-N (magenta). Note the flipped binding mode of the indole ring but maintenance of the hydrogen bond from the indole nitrogen to the backbone of Val56.

similar to the structure of 1F1 bound to pepstatin:PR with respect to the protein (rmsd 0.19 Å, Supplemental Table 3), but interestingly, the binding mode of 1F1-N is flipped, with the orientation of the indole ring inverted relative to the binding of 1F1, as predicted by AutoDock (Figure 3; Supplemental Figure 5). This places the carboxylic acid groups in the same general orientation relative to the protein for both 1F1 and 1F1-N and preserves all of the key interactions with PR. Hydrophobic interactions with Trp42, Pro 44, Met 46, and Lys55 are maintained; the indole nitrogen forms a hydrogen bond with the carbonyl of Val56; and an electrostatic interaction occurs with Arg57. The observed binding mode of the indole ring corresponds closely to that predicted by AutoDock (Supplemental Figure S5a), while two alternate conformations with comparable cluster size are predicted for the propionic acid side chain: one with the carboxyl group oriented toward Lys55 and one with the carboxyl group interacting with Arg57 (Supplemental Figure 5b). The latter pose is similar to that observed in the crystal structure (Supplemental Figure 5a), with the carboxylic acid moiety at a distance of 4.9 Å from the guanidinium group of Arg57.

Apo-PR with 1F1-N. The structure of 1F1-N bound to autolysis-resistant apo-PR was obtained from rod-like $P2_12_12_1$ crystals to 2.0 Å (Table 1; Supplemental Table 1; Figure 4) and is similar to the structures of 1F1 and 1F1-N bound to pepstatin:PR (rmsd ≈ 0.8 Å, Supplemental Table 3); *i.e.*, the flaps are in a closed conformation. As in the structure of apo−PR with 1F1, the active site is occupied only by a handful of solvent molecules (Supplemental Figure 4). However, here the flaps have the usual handedness, unlike the structure of apo−PR with 1F1 in which the inner and outer flaps are switched. 1F1-N occupies a virtually identical position in the cocrystal structures with apo−PR and pepstatin:PR (Figure 4).

Protease Conformation. Flap mobility in HIV PR has been examined by NMR, double electron−electron resonance (DEER), pulse-EPR spectroscopy with nitroxide spin-labels, and MD simulations.[22−30] These studies indicate that individual flaps in the native protein sample several different conformations, including closed, open or closed with inverted flaps, semiopen, and wide-open, with the majority of the protein (60−80% depending on subtype/mutations[27]) being in the semiopen state. DEER profiles are significantly shifted to favor the closed state with the addition of active-site PR inhibitors.[28] Of 270 structures of HIV protease in the PDB, the only apo structures in the closed conformation are of tethered dimers.[31−35] The only other known apo-PR crystal structures either have flaps in an open or semiopen conformation stabilized by lattice contacts, or the flaps are disordered.[18] The structures of apo-PR with 1F1 and 1F1-N bound are notable for being the first crystal structures of apo-PR with closed flaps (see Supplemental Figure 8; further discussion in Supporting Information) and suggest that the binding of compounds in the flap site favors a closed flap conformation of the protease in solution.

Comparison of the pepstatin-bound structures of PR:acetyl-pepstatin (5HVP[19]), PR:pepstatin:1F1, and PR:pepstatin:1F1-N reveals nearly identical interactions with pepstatin in the active site. The most significant differences among these structures are observed in the conformation of the weakly ordered 34−41 loop (ear) on chain B when the fragment binds in the flap site of chain A. Additionally, the side chain of Lys55 in the A chain, which adopts a conformation blocking the flap site, is displaced when fragments are bound (Supplemental Figure 6).

An additional unusual feature of these structures is crystallization in the $P2_12_12_1$ space group with unit cell dimensions of ∼28, 65, and 92 Å. Twelve structures of HIV PR are deposited in the PDB in this space group (4FAE, 4FAF, 3UFN, 3S53, 3S56, 3SO9, 2HS1, 2HS2, 1Z8C, 1NHO, 3KFR, and 3KFS). Nine of these are complexes with flap site binders.[8,16,36] Inspection of the electron density maps of the remaining three indicates unmodeled or poorly modeled electron density in the flap site (for further discussion, see Supporting Information). Thus, crystallization of HIV PR in the $P2_12_12_1$ crystal form is an indicator of binding in the flap site in that the bound conformation is unique and favors this particular packing arrangement.

Differential Scanning Fluorimetry. To confirm that the interactions of 1F1 and 1F1-N observed in crystals also occur in solution, DSF curves were measured with varying concentrations of 1F1 and 1F1-N with autolysis-resistant apo−PR. In both cases, the compounds increased the thermal stability of HIV PR in a concentration-dependent manner, indicating protein−ligand binding.[37,38] At 5 mM, 1F1 increases the melting temperature of apo HIV PR by 5 °C, while 1F1-N increases the melting temperature of apo HIV PR by 3.5 °C

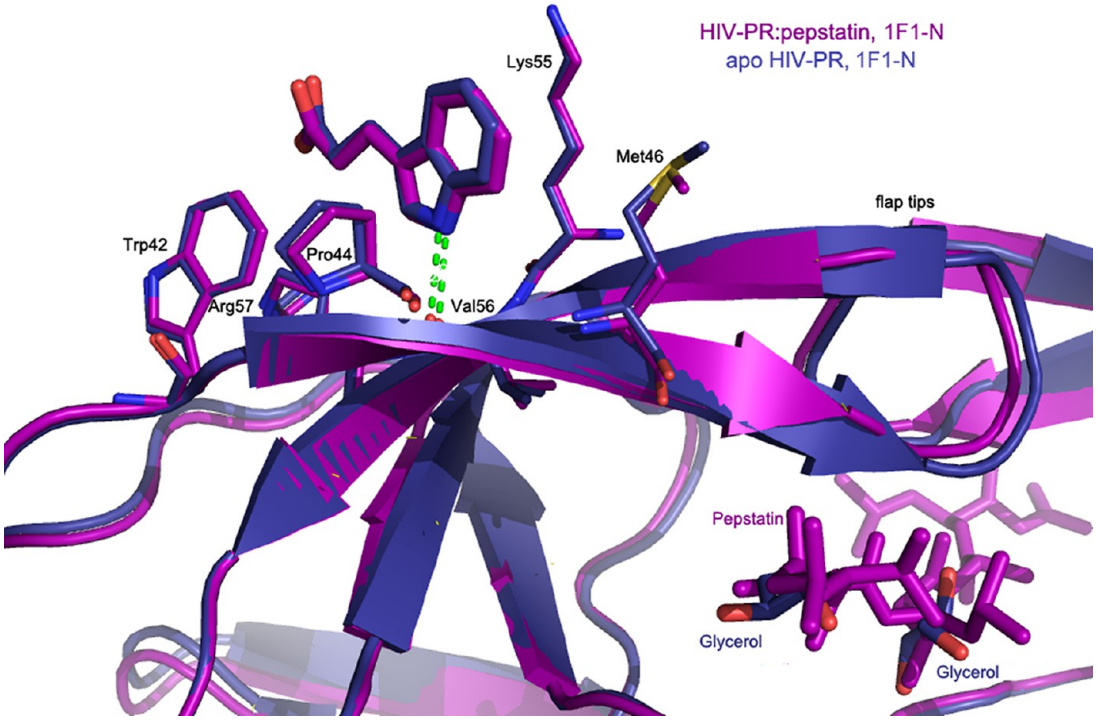

Figure 4. Structure of HIV PR:pepstatin bound to 1F1-N (magenta) compared to the structure of apo HIV PR bound to 1F1-N (navy).

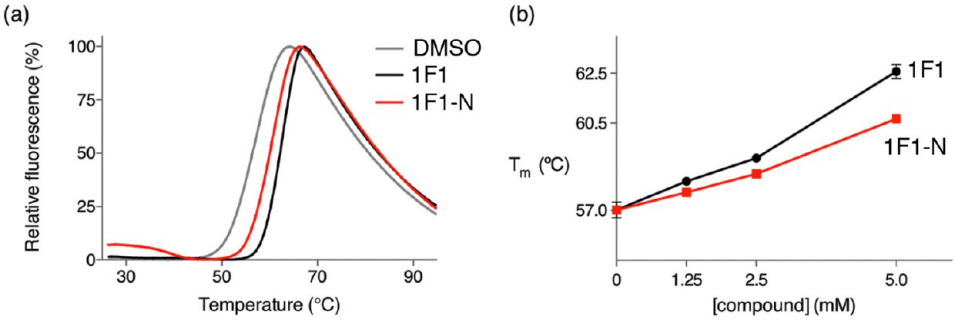

Figure 5. Differential scanning fluorimetry of apo, autolysis resistant HIV PR in the presence and absence of fragments showing that 1F1 and 1F1-N stabilize the protease in solution, consistent with binding in the site observed in crystal structures and flap closure. (a) The presence of 5 mM 1F1 and 1F1-N increases the melting temperature of protease, as indicated by shifts in the DSF curves. (b) 1F1 and 1F1-N stabilize protease in a dose-dependent manner.

(Figure 5). As a control, DSF experiments were performed on selected compounds from the 22-member library, and stabilizing temperature shifts were not observed (Supplemental Figure 7a). However, DSF was not a useful tool to narrow down potential binding because the background fluorescence of a number of the compounds was too high to obtain reliable results. For example, two fragments that inhibited crystal nucleation, 1F1-E and 1F1-F, exhibited levels of fluorescence that overwhelmed the DSF signal at the required millimolar concentrations (Supplemental Figure 7b). The larger shift caused by 1F1 is consistent with the hydrogen bonds with Arg57 observed in the 1F1 complexes compared to the longer range electrostatic interaction in the 1F1-N complexes. Thermal stabilization via fragments interacting with residues in the flap site is consistent with MD simulations, which identify conserved, noncovalent interactions that couple secondary structure elements within the tertiary structure of the PR dimer.[39]

Back-Scattering Interferometry. To further investigate the binding of 1F1 and 1F1-N to HIV PR in solution, backscattering interferometry (BSI) was performed on samples of apo−PR and pepstatin:PR with both compounds. BSI detects changes in refractive index upon binding that can be used to determine K_d from dose−response measurements.[40−44] The signal detected in a BSI measurement is the maximal refractive index change upon binding of a solute to a dilute protein solution. Both 1F1 and 1F1-N were tested with apo−PR and pepstatin:PR (Figure 6). The K_d values for both fragments are in the low micromolar range and within experimental error both with and without pepstatin. The results indicate that fragment binding can occur when pepstatin is bound and the flap is constrained to a closed conformation. Further, the results show that fragments bind equally well to apo−PR in which the flaps can adopt a range of conformations. Interestingly, the maximal change in phase change, which is a measure of the extent of overall conformational change, was greater in the absence of pepstatin, indicating a larger change in

dx.doi.org/10.1021/cb300611p | ACS Chem. Biol. 2013, 8, 1223−1231

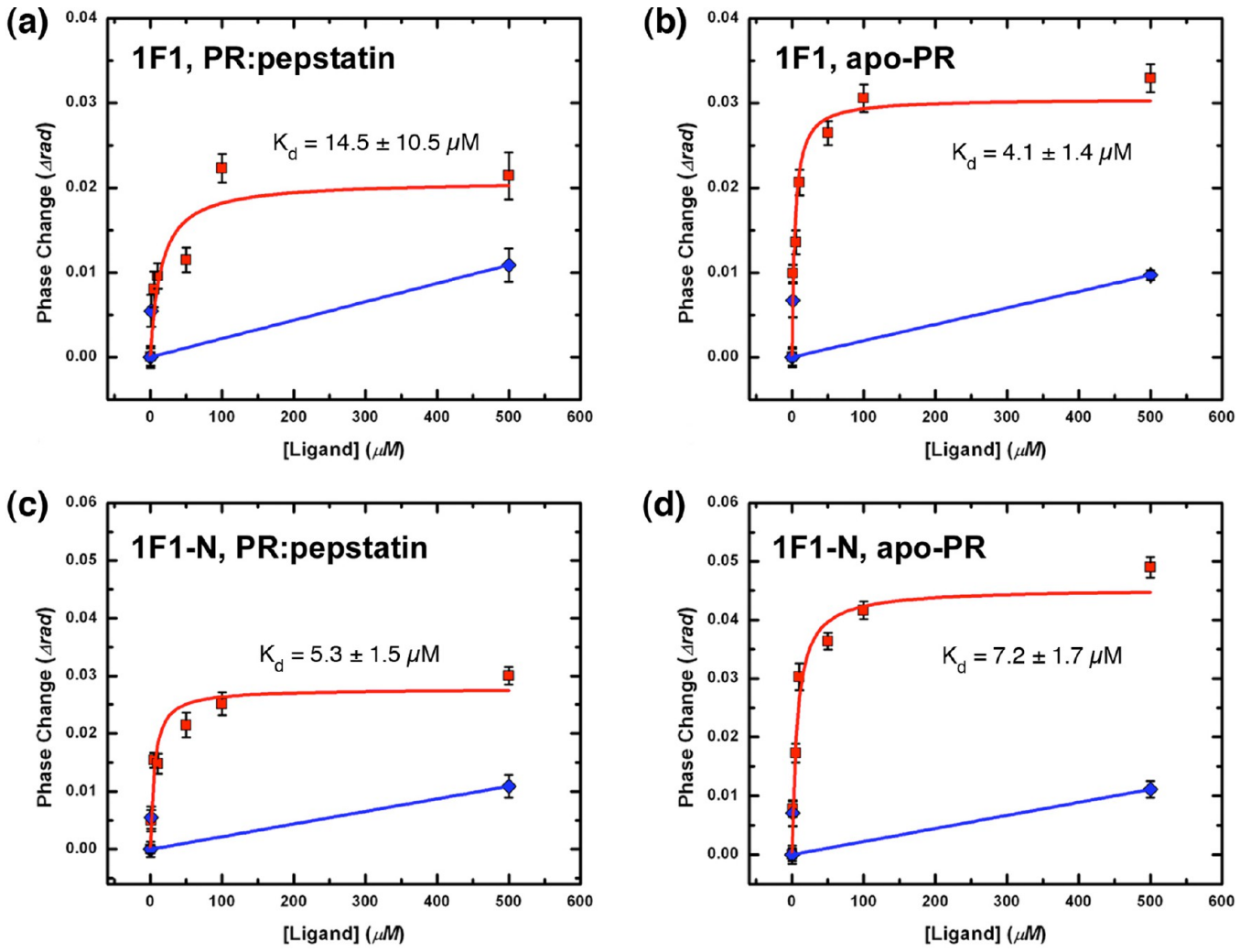

Figure 6. Backscattering interferometry for (a) AR-PR:pepstatin + 1F1, (b) apo−PR + 1F1, (c) AR-PR:pepstatin + 1F1-N, and (d) apo-PR + 1F1-N. Note that all K_d values are equal within experimental error, but the phase change is significantly greater for compound binding to apo-PR.

conformation of the protein upon compound binding.[45] The difference in effective concentrations (mM for DSF and μM for BSI) reflects the nature of the different assays. It is worth noting that the DSF assay was performed with 5% DMSO, while BSI had 1% DMSO. Stabilization of protein to thermal-induced motion requires a much greater degree of site occupancy, so DSF reports on saturating concentrations. In contrast, BSI signals are generated in proportion to binding site occupancy, giving a true K_d value for a given compound; however, it is also possible that additional binding sites other than the crystallographic binding site are occupied under these conditions. Note that the label-free nature of BSI is necessary for such small molecules as 1F1 and 1F1-N: the addition of any label other than a radioisotope would significantly change the properties of the compounds.

HIV Protease Activity Assay. Inhibition of PR activity by 1F1 and 1F1-N was tested using a fluorogenic peptide substrate. The fluorescence of 1F1 overwhelms the signal of the assay at high micromolar concentrations. No significant inhibition of PR was observed for 1F1-N up to 1 mM; nor was a significant increase observed for the inhibition of PR by pepstatin in the presence of 1F1-N (Supplemental Tables 5, 6). However, our long-term goal is to develop larger, higher affinity compounds from these fragment-like starting points. Growing these fragments will enable additional contacts with the protein, increasing their potential for inhibition. Since it is also possible that the 1F1 binding site is involved in protein−protein interactions, larger derivatives may show effects in more sophisticated assays using full-length Gag domains.

Fragment-Optimization and Future Directions. The common structural features arising from different binding modes of 1F1 and 1F1-N can be exploited to design larger molecules. The hydrophobic core of the fragments is stabilized by hydrophobic and van der Waals interactions with Trp42, Pro44, and Lys55 side chains, while its orientation depends on the hydrogen bond acceptor−donor pattern with Val56 and Arg57, respectively (Figure 7). This binding mode places the molecules along a groove roughly delimited by Met46 and Pro79, defining two main directions where molecules can be grown to further stabilize current interactions and possibly extend the compound's interaction network.

Both fragments establish a single hydrogen bond with Arg57, suggesting that the carboxyl moiety could be esterified while keeping the key hydrogen bond. Larger groups could reach and engage the cavity enclosed by Arg57, Glu35, and Pro79. An opportune hydrogen bond donor here could also help establish a directional interaction with Glu35, contributing to destabilization of its salt bridge with Arg57. On the other side of the

dx.doi.org/10.1021/cb300611p | ACS Chem. Biol. 2013, 8, 1223−1231

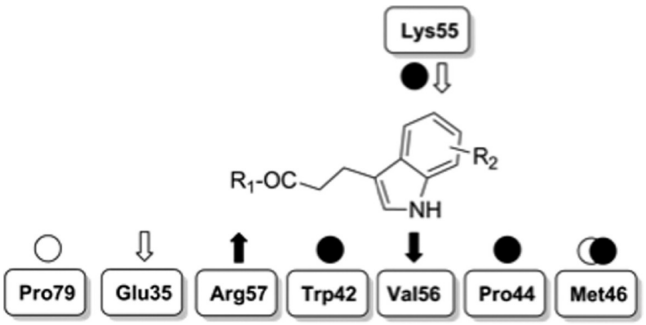

Figure 7. Schematic representation of essential interactions identified in the crystallographic structures and potentially exploitable ones. Experimental interactions are tagged with filled arrows and circles; interactions exploitable by chemical derivatives are shown with empty arrows and circles. Arrows = h-bonds; circles = vdW interactions.

groove, hydrogen bonding with Val56 orients the fragment's aromatic rings so they interact with Pro44, Lys55, and Met46. Substituents on the rings could be used to extend contacts with these residues. In particular, a hydrogen bond acceptor group could interact with the amino group of Lys55, strengthening the binding. Additionally, hydrophobic groups could further extend the molecules toward Met46, increasing close contacts and stabilizing its side chain.

Such modifications could improve overall binding and might lead to a compound with observable protease inhibition activity. Also, since Pro79 is fairly close to the active site (i.e., approximately 10 Å away from one of the benzyl groups of TL-3), molecular hybrids linking 1F1-site binders and active site inhibitors could be designed to test the hypothesis of cooperative binding.

CONCLUSIONS

Allosteric regulation of HIV protease activity is a novel potential way to limit the development of drug-resistance. We show here that indole-carboxylate small molecules occupy an external site on the protease in both the solid state (by X-ray crystallography) and in solution (by measurements of conformational stabilization and direct site occupancy). Future work will focus on expanding these molecules into larger compounds with observable inhibition of PR.

METHODS

Expression and Purification. Cloning of wild-type NL4-3 HIV-1 PR was described previously.[46] The autolysis-resistant HIV-1 protease (Q7K, L33I, L63I, C67A, and C95A),[20] used for apo structures, was constructed using multiple rounds of the QuikChange site-directed mutagenesis protocol. For both variants, protein expression was induced in *E. coli*. Inclusion bodies were isolated by centrifugation, solubilized, and purified by ion-exchange chromatography and FPLC. PR was dialyzed against 10 mM sodium acetate buffer, pH 5.2, and 0.1% 2-mercaptoethanol prior to filtration and concentration to 3−5 mg mL^{-1}. The purified PR was separated using SDS-PAGE, and purity was verified by Western blot using rabbit antiserum against HIV PR. For further details, see Supporting Information.

***In Silico* Docking.** The structural features of 1F1 were used to search for potential derivatives to be screened by molecular docking. The ZINC online database (version 11)[47] was filtered for compounds containing both the benzindole ring and at least one carboxylic acid group. The results of this first filtering round were refined by rejecting molecules that do not have the properties of a fragment hit[48] (MW ≤ 300; HB donors ≤ 3; HB acceptors ≤ 6), leading to a set of 2499 commercially available compounds. Finally, this set was prepared with AutoDockIRaccoon (available online at http://autodock.scripps.edu/resources/raccoon) and docked with AutoDock v4.2[17] on the HIV protease monomer bound to 1F1 (PDB_id 3KFR, chain B). Docking results were ranked and filtered by using 1F1 docking score (−5.57 kcal mol^{-1}) and ligand efficiency (−0.43) as references. Ligands with docking score of −4.50 kcal mol^{-1} or better were visually inspected to obtain a list of the top 45 hits, and 22 of them were purchased and submitted to crystallization-based screening. For further details, see Supporting Information.

Crystallization and Data Collection. Crystallization was performed by vapor-diffusion in 96-well or 24-well plates at 18 °C. For all cocrystallization experiments, protein samples were prepared by adding 10% of a 200 mM solution of the compound of interest in DMSO to the protein sample. For the inhibited forms of PR, pepstatin or TL-3 were added prior to the addition of the compound. Screens of apo−PR were always conducted using the autolysis-resistant variant. Samples were centrifuged to remove any insoluble inhibitor or compound prior to crystallization. Crystallization conditions were obtained using commercially available 96-well screens. Conditions for each of the crystal forms are summarized in Table 1. For further details of cryoprotection, data collection, and data processing, see Supporting Information.

Differential Scanning Fluorimetry. Differential scanning fluorimetry (DSF) measurements were taken using a LightCycler 480 Real-Time PCR System (Roche) using 465 nm excitation and 580 nm emission wavelengths. The temperature was increased from 25 to 95 °C at a rate of 0.06 °C/s, with 10 acquisitions/°C. Samples were loaded into white 96-well plates. Each well contained a total volume of 20 μL consisting of 4 μM apo−PR, 10 mM HEPES at pH 7.5, 150 mM NaCl, 20× SYPRO Orange (Invitrogen), and 5% DMSO. Melting temperature calculations were carried out using the LightCycler 480 Protein Melting Software (Roche).

Backscattering Interferometry. All experiments were performed in Dulbecco's Phosphate Buffered Saline (pH 7.4) with 1% (v/v) DMSO. Samples of apo−PR (2 μM) were incubated in the presence and absence of fixed concentrations of pepstatin (4.8 μM) and varying concentrations of small molecule ligands (1F1, 1F1-N, and tryptophan) for 1 h at 20 °C. Samples were then deposited into the channels of a microfluidic chip for analysis using a custom-built backscattering interferometer (BSI). Microfluidic chip surfaces were regenerated between uses by brief rinsing with a 3:2 solution of methanol and deionized water. The microfluidic devices were maintained at 25 °C using a feedback-controlled peltier system. The high contrast interference fringes produced by each sample were generated using a fiber-coupled HeNe laser and recorded on a CCD camera. Measurements were analyzed using a combination of in-house software, Microsoft Excel, and OriginPro.

ASSOCIATED CONTENT

Supporting Information

Refinement statistics, chemical structures, rmsd comparisons, AutoDock binding modes, FRET-based inhibition results, electron density. This material is available free of charge via the Internet at http://pubs.acs.org.

Accession Codes

Coordinates and structure factors have been deposited in the Protein Data Bank with accession numbers 4EJ8, 4EJD, 4EJK, and 4EJL.

AUTHOR INFORMATION

Corresponding Author

*(T.T.) Phone: 858-784-2110. Fax: 858-784-2857. E-mail: theresat@scripps.edu.

Notes

The authors declare no competing financial interest.

■ ACKNOWLEDGMENTS

This research was supported by Program Project grant P01 GM083658-05 from the National Institutes of Health, National Institute for General Medical Sciences. T.T. was funded by the Molecular Basis of Viral Pathogenesis Training Grant, 2T32AI007354. Assistance provided by the support staff at the Stanford Synchrotron Radiation Lightsource (SSRL) for data collection is greatly appreciated. We thank the Scripps High-Performance Computing for the support provided to Garibaldi HPC Linux cluster. Portions of this research were carried out at the Stanford Synchrotron Radiation Lightsource, a Directorate of SLAC National Accelerator Laboratory and an Office of Science User Facility operated for the U.S. Department of Energy Office of Science by Stanford University. The SSRL Structural Molecular Biology Program is supported by the DOE Office of Biological and Environmental Research and by the National Institutes of Health, National Center for Research Resources, Biomedical Technology Program (P41RR001209), and the National Institute of General Medical Sciences.

■ REFERENCES

(1) Wheeler, W. H., Ziebell, R. A., Zabina, H., Pieniazek, D., Prejean, J., Bodnar, U. R., Mahle, K. C., Heneine, W., Johnson, J. A., and Hall, H. I. (2010) Prevalence of transmitted drug resistance associated mutations and HIV-1 subtypes in new HIV-1 diagnoses, U.S.-2006. *AIDS 24*, 1203−1212.

(2) UNAIDS. (2010) *UNAIDS report on the global AIDS epidemic 2010*, Joint United Nations Programme on HIV/AIDS (UNAIDS), Geneva, Switzerland.

(3) Shen, L., and Siliciano, R. F. (2008) Viral reservoirs, residual viremia, and the potential of highly active antiretroviral therapy to eradicate HIV infection. *J. Allergy. Clin. Immunol. 122*, 22−28.

(4) Ali, A., Bandaranayake, R. M., Cai, Y., King, N. M., Kolli, M., Mittal, S., Murzycki, J. F., Nalam, M. N., Nalivaika, E. A., Ozen, A., Prabu-Jeyabalan, M. M., Thayer, K., and Schiffer, C. A. (2011) Molecular basis for drug resistance in HIV-1 protease. *Viruses 2*, 2509−2535.

(5) Wensing, A. M., van Maarseveen, N. M., and Nijhuis, M. (2009) Fifteen years of HIV protease inhibitors: raising the barrier to resistance. *Antiviral Res. 85*, 59−74.

(6) De Clercq, E. (1999) Perspectives of non-nucleoside reverse transcriptase inhibitors (NNRTIs) in the therapy of HIV-1 infection. *Farmaco 54*, 26−45.

(7) Lee, G. M., and Craik, C. S. (2009) Trapping moving targets with small molecules. *Science 324*, 213−215.

(8) Kovalevsky, A. Y., Liu, F., Leshchenko, S., Ghosh, A. K., Louis, J. M., Harrison, R. W., and Weber, I. T. (2006) Ultra-high resolution crystal structure of HIV-1 protease mutant reveals two binding sites for clinical inhibitor TMC114. *J. Mol. Biol. 363*, 161−173.

(9) Kovalevsky, A. Y., Ghosh, A. K., and Weber, I. T. (2008) Solution kinetics measurements suggest HIV-1 protease has two binding sites for darunavir and amprenavir. *J. Med. Chem. 51*, 6599−6603.

(10) Kovalevsky, A. Y., Louis, J. M., Aniana, A., Ghosh, A. K., and Weber, I. T. (2008) Structural evidence for effectiveness of darunavir and two related antiviral inhibitors against HIV-2 protease. *J. Mol. Biol. 384*, 178−192.

(11) Prabu-Jeyabalan, M., Nalivaika, E., and Schiffer, C. A. (2002) Substrate shape determines specificity of recognition for HIV-1 protease: analysis of crystal structures of six substrate complexes. *Structure 10*, 369−381.

(12) Nalam, M. N., Ali, A., Altman, M. D., Reddy, G. S., Chellappan, S., Kairys, V., Ozen, A., Cao, H., Gilson, M. K., Tidor, B., Rana, T. M., and Schiffer, C. A. (2010) Evaluating the substrate-envelope hypothesis: structural analysis of novel HIV-1 protease inhibitors designed to be robust against drug resistance. *J. Virol. 84*, 5368−5378.

(13) Perryman, A. L., Lin, J. H., and McCammon, J. A. (2004) HIV-1 protease molecular dynamics of a wild-type and of the V82F/I84V mutant: Possible contributions to drug resistance and a potential new target site for drugs. *Protein Sci. 13*, 1108−1123.

(14) Azam, M., Powers, J. T., Einhorn, W., Huang, W. S., Shakespeare, W. C., Zhu, X., Dalgarno, D., Clackson, T., Sawyer, T. K., and Daley, G. Q. (2010) AP24163 inhibits the gatekeeper mutant of BCR-ABL and suppresses *in vitro* resistance. *Chem. Biol. Drug Des. 75*, 223−227.

(15) Zhang, J., Adrian, F. J., Jahnke, W., Cowan-Jacob, S. W., Li, A. G., Iacob, R. E., Sim, T., Powers, J., Dierks, C., Sun, F., Guo, G. R., Ding, Q., Okram, B., Choi, Y., Wojciechowski, A., Deng, X., Liu, G., Fendrich, G., Strauss, A., Vajpai, N., Grzesiek, S., Tuntland, T., Liu, Y., Bursulaya, B., Azam, M., Manley, P. W., Engen, J. R., Daley, G. Q., Warmuth, M., and Gray, N. S. (2010) Targeting Bcr-Abl by combining allosteric with ATP-binding-site inhibitors. *Nature 463*, 501−506.

(16) Perryman, A. L., Zhang, Q., Soutter, H. H., Rosenfeld, R., McRee, D. E., Olson, A. J., Elder, J. E., and Stout, C. D. (2010) Fragment-based screen against HIV protease. *Chem. Biol. Drug Des. 75*, 257−268.

(17) Morris, G. M., Huey, R., Lindstrom, W., Sanner, M. F., Belew, R. K., Goodsell, D. S., and Olson, A. J. (2009) AutoDock4 and AutoDockTools4: Automated docking with selective receptor flexibility. *J. Comput. Chem. 30*, 2785−2791.

(18) Heaslet, H., Rosenfeld, R., Giffin, M., Lin, Y.-C., Tam, K., Torbett, B. E., Elder, J. H., McRee, D. E., and Stout, C. D. (2007) Conformational flexibility in the flap domains of ligand-free HIV protease. *Acta Crystallogr., Sect. D: Biol. Crystallogr. 63*, 866−875.

(19) Fitzgerald, P. M., McKeever, B. M., VanMiddlesworth, J. F., Springer, J. P., Heimbach, J. C., Leu, C. T., Herber, W. K., Dixon, R. A., and Darke, P. L. (1990) Crystallographic analysis of a complex between human immunodeficiency virus type 1 protease and acetyl-pepstatin at 2.0-A resolution. *J. Biol. Chem. 265*, 14209−14219.

(20) Mildner, A. M., Rothrock, D. J., Leone, J. W., Bannow, C. A., Lull, J. M., Reardon, I. M., Sarcich, J. L., Howe, W. J., Tomich, C. S., Smith, C. W., et al. (1994) The HIV-1 protease as enzyme and substrate: mutagenesis of autolysis sites and generation of a stable mutant with retained kinetic properties. *Biochemistry 33*, 9405−9413.

(21) Scott, W. R., and Schiffer, C. A. (2000) Curling of flap tips in HIV-1 protease as a mechanism for substrate entry and tolerance of drug resistance. *Structure 8*, 1259−1265.

(22) Katoh, E., Louis, J. M., Yamazaki, T., Gronenborn, A. M., Torchia, D. A., and Ishima, R. (2003) A solution NMR study of the binding kinetics and the internal dynamics of an HIV-1 protease-substrate complex. *Protein Sci. 12*, 1376−1385.

(23) Freedberg, D. I., Ishima, R., Jacob, J., Wang, Y. X., Kustanovich, I., Louis, J. M., and Torchia, D. A. (2002) Rapid structural fluctuations of the free HIV protease flaps in solution: Relationship to crystal structures and comparison with predictions of dynamics calculations. *Protein Sci. 11*, 221−232.

(24) Ishima, R., Freedberg, D. I., Wang, Y. X., Louis, J. M., and Torchia, D. A. (1999) Flap opening and dimer-interface flexibility in the free and inhibitor-bound HIV protease, and their implications for function. *Struct. Folding Des. 7*, 1047−1055.

(25) Galiano, L., Bonora, M., and Fanucci, G. E. (2007) Interflap distances in HIV-1 protease determined by pulsed EPR measurements. *J. Am. Chem. Soc. 129*, 11004−11005.

(26) Ding, F., Layten, M., and Simmerling, C. (2008) Solution structure of HIV-1 protease flaps probed by comparison of molecular dynamics simulation ensembles and EPR experiments. *J. Am. Chem. Soc. 130*, 7184−7185.

(27) Kear, J. L., Blackburn, M. E., Veloro, A. M., Dunn, B. M., and Fanucci, G. E. (2009) Subtype polymorphisms among HIV-1 protease variants confer altered flap conformations and flexibility. *J. Am. Chem. Soc. 131*, 14650−14651.

(28) Blackburn, M. E., Veloro, A. M., and Fanucci, G. E. (2009) Monitoring inhibitor-induced conformational population shifts in HIV-1 protease by pulsed EPR spectroscopy. *Biochemistry 48*, 8765−8767.

(29) Torbeev, V. Y., Raghuraman, H., Hamelberg, D., Tonelli, M., Westler, W. M., Perozo, E., and Kent, S. B. (2011) Protein conformational dynamics in the mechanism of HIV-1 protease catalysis. *Proc. Natl. Acad. Sci. U.S.A. 108*, 20982−20987.
(30) Torbeev, V. Y., Raghuraman, H., Mandal, K., Senapati, S., Perozo, E., and Kent, S. B. (2009) Dynamics of "flap" structures in three HIV-1 protease/inhibitor complexes probed by total chemical synthesis and pulse-EPR spectroscopy. *J. Am. Chem. Soc. 131*, 884−885.
(31) Pillai, B., Kannan, K. K., and Hosur, M. V. (2001) 1.9 A X-ray study shows closed flap conformation in crystals of tethered HIV-1 PR. *Proteins 43*, 57−64.
(32) Das, A., Mahale, S., Prashar, V., Bihani, S., Ferrer, J. L., and Hosur, M. V. (2010) X-ray snapshot of HIV-1 protease in action: observation of tetrahedral intermediate and short ionic hydrogen bond SIHB with catalytic aspartate. *J. Am. Chem. Soc. 132*, 6366−6373.
(33) Kumar, M., Kannan, K. K., Hosur, M. V., Bhavesh, N. S., Chatterjee, A., Mittal, R., and Hosur, R. V. (2002) Effects of remote mutation on the autolysis of HIV-1 PR: X-ray and NMR investigations. *Biochem. Biophys. Res. Commun. 294*, 395−401.
(34) Mittal, S., Cai, Y., Nalam, M. N. L., Bolon, D. N. A., and Schiffer, C. A. (2012) Hydrophobic core flexibility modulates enzyme activity in HIV-1 protease. *J. Am. Chem. Soc. 134*, 4163−4168.
(35) Bihani, S. C., Das, A., Prashar, V., Ferrer, J. L., and Hosur, M. V. (2009) Resistance mechanism revealed by crystal structures of unliganded nelfinavir-resistant HIV-1 protease non-active site mutants N88D and N88S. *Biochem. Biophys. Res. Commun. 389*, 295−300.
(36) Brynda, J., Rezacova, P., Fabry, M., Horejsi, M., Stouracova, R., Sedlacek, J., Soucek, M., Hradilek, M., Lepsik, M., and Konvalinka, J. (2004) A phenylnorstatine inhibitor binding to HIV-1 protease: a geometry, protonation, and subsite−pocket interactions analyzed at atomic resolution. *J. Med. Chem. 47*, 2030−2036.
(37) Vedadi, M., Niesen, F. H., Allali-Hassani, A., Fedorov, O. Y., Finerty, P. J., Jr., Wasney, G. A., Yeung, R., Arrowsmith, C., Ball, L. J., Berglund, H., Hui, R., Marsden, B. D., Nordlund, P., Sundstrom, M., Weigelt, J., and Edwards, A. M. (2006) Chemical screening methods to identify ligands that promote protein stability, protein crystallization, and structure determination. *Proc. Natl. Acad. Sci. U.S. A. 103*, 15835−15840.
(38) Niesen, F. H., Berglund, H., and Vedadi, M. (2007) The use of differential scanning fluorimetry to detect ligand interactions that promote protein stability. *Nat. Protoc. 2*, 2212−2221.
(39) Rücker, P., Horn, A., Meiselbach, H., and Sticht, H. (2011) A comparative study of HIV-1 and HTLV-I protease structure and dynamics reveals a conserved residue interaction network. *J. Mol. Model. 17*, 2693−2705.
(40) Bornhop, D. J., Latham, J. C., Kussrow, A., Markov, D. A., Jones, R. D., and Sorensen, H. S. (2007) Free-solution, label-free molecular interactions studied by back-scattering interferometry. *Science 317*, 1732−1736.
(41) Latham, J. C., Stein, R. A., Bornhop, D. J., and McHaourab, H. S. (2009) Free-solution label-free detection of alpha-Crystallin chaperone interactions by back-scattering interferometry. *Anal. Chem. 81*, 1865−1871.
(42) Baksh, M. M., Kussrow, A. K., Mileni, M., Finn, M. G., and Bornhop, D. J. (2011) Label-free quantification of membrane-ligand interactions using backscattering interferometry. *Nat. Biotechnol. 29*, 357−360.
(43) Kussrow, A., Baksh, M. M., Bornhop, D. J., and Finn, M. G. (2011) Universal sensing by transduction of antibody binding with backscattering interferometry. *ChemBioChem 12*, 367−370.
(44) Kussrow, A., Enders, C. S., and Bornhop, D. J. (2011) Interferometric methods for label-free molecular interaction studies. *Anal. Chem. 84*, 779−792.
(45) Olmsted, I. R., Xiao, Y., Cho, M., Csordas, A. T., Sheehan, J. H., Meiler, J., Soh, H. T., and Bornhop, D. J. (2011) Measurement of aptamer−protein interactions with back-scattering interferometry. *Anal. Chem. 83*, 8867−8870.
(46) Buhler, B., Lin, Y. C., Morris, G., Olson, A. J., Wong, C. H., Richman, D. D., Elder, J. H., and Torbett, B. E. (2001) Viral evolution in response to the broad-based retroviral protease inhibitor TL-3. *J. Virol. 75*, 9502−9508.
(47) Irwin, J. J., and Shoichet, B. K. (2005) ZINC: a free database of commercially available compounds for virtual screening. *J. Chem. Inf. Model. 45*, 177−182.
(48) Congreve, M., Carr, R., Murray, C., and Jhoti, H. (2003) A 'rule of three' for fragment-based lead discovery? *Drug Discovery Today 8*, 876−877.

NOTE ADDED AFTER ASAP PUBLICATION

This paper was published ASAP on March 29, 2013 with an incorrect Supporting Information file. The reference to the Supporting Information in the section titled HIV Protease Activity Assay has been updated, as well. The revised version was re-posted on June 11, 2013.